Wind and Structures, *Vol. 28, No. 3 (2019) 191-201*
DOI: https://doi.org/10.12989/was.2019.28.3.191

Numerical optimization of a vertical axis wind turbine: case study at TMU campus

Seyed Kourosh Mirfazli[1a], Mohammad Hossein Giahi[2b] and Ali Jafarian Dehkordi[*1]

[1]*School of Mechanical Engineering, Tarbiat Modares University, Jalal Ale Ahmad Highway, Tehran, Iran*
[2]*School on Mechanical Engineering, Saskatchewan University, 69 Campus Dr, Saskatoon, SK, Canada*

(Received February 4, 2018, Revised December 27, 2018, Accepted December 28, 2018)

Abstract. In this paper, the aerodynamic analysis of a vertical axis wind turbine was carried out by CFD approach to optimize the turbine performance. To perform numerical simulation, SST-Transition turbulence model was used, which demonstrated more precise results compared to non-transition models. A parametric study was conducted to optimize the VAWT performance based on the selected model. The investigation of pitch angle changes showed that the highest power produced by the turbine occurs at 2° angle. Considering the effect of the rotor's arm junction to the airfoil showed that by increasing the distance of the junction from the edge of the airfoil from 25 cm to 40 cm, the power of the turbine increases by 60%. However, further increase in this distance results in power decrease. Based on the proposed numerical model, a case study was conducted to consider the installation of four VAWTs in the southwest corner of the medical science building at TMU campus with a height of 42m. The results of the simulation showed that 8.27 MWh energy is obtainable annually.

Keywords: vertical axis wind turbine; CFD simulation; turbulence models; case study

1. Introduction

As global energy demand continues to grow, the ability of traditional sources of energy such as fossil fuels to satisfy this demand is decreasing (Soto and Jentsch 2016). Wind energy is among the renewable energy sources which has great potential to produce electrical power; however, further research is needed to improve the performance of wind turbines (Cooney *et al.* 2017). Wind turbines are generally classified as two types: horizontal axis and vertical axis turbines. This classification refers to the position of rotor axis relative to wind (Dobrev and Massouh 2011). Small-scale vertical-axis wind-turbines are a popular source of power in urban areas, providing residential electricity and the ability to generate power regardless of the direction of the wind (Lin *et al.* 2016). To enhance vertical axis wind turbine technology, several studies have been conducted in recent years.

Several methods have been purposed to model the flow in VAWTs and predict the turbine performance. Marini *et al.* (1992) compared the aerodynamic performance of VAWTs using two models: single stream tube momentum model and free wake vortex model. The results showed that the momentum model predicts the VAWT performance in a simple and fairly accurate way. The vortex model was also used in another study by Islam *et al.* (2008) in conjunction with double-multiple streamtube and cascade models. These models were used for performance prediction and design of straight-bladed VAWTs. Among these three models, vortex model is considered to be the most accurate model, although computationally expensive. It was also found that the double-multiple streamtube model is not suitable for high tip speed ratios. They concluded that the cascade model gives smooth convergence even in high tip speed ratios with reasonable accuracy.

Howell *et al.* (2010) presented a combined experimental and computational procedure to study the aerodynamics and performance of a small scale vertical axis wind turbine. Wind tunnel tests as well as two and three-dimensional unsteady CFD simulations were carried out to investigate the overall performance of the turbine. It is shown experimentally that the surface roughness of the turbine blades has a strong influence on performance. Both two bladed and three bladed rotors were tested and a significant increase in performance coefficient is observed for three bladed rotors. Another numerical and experimental study of Darrieus-type VAWT was done by Lee and Lim (2015). The study proposed an optimum turbine shape which produced maximum output power. The results showed that, as solidity increases, power coefficient grows in low tip speed ratio (TSR) range. However, in high tip speed ratios, as the rotational speed increases, the drag force also grows. Consequently, a model with high solidity produces a low power coefficient because it is affected by stronger drag force.

The performance of a novel vertical axis wind turbine was investigated using RANS CFD simulations by McTavish *et al*. (2012). Computational investigation of the torque characteristics of the novel rotor was conducted using commercial computational fluid dynamics software. Steady two-dimensional CFD simulations were conducted

*Corresponding author, Associate Professor
E-mail: jafarian@modares.ac.ir
[a] M.Sc.
E-mail: Seyedkourosh.mirfazli@modares.ac.ir
[b] Ph.D. Student
E-mail: mh.giahi@usask.ca

ISSN: 1226-6116 (Print), 1598-6225 (Online)

and it was determined that the novel rotor configuration produces an amount of static torque comparable with those of existing rotors. Similarly, Zamani *et al*. (2016) studied a new approach to improve VAWTs performance and torque by suggesting a novel turbine shape. J-shaped profiles were used in the structure of blades by eliminating the pressure side of airfoil which results in a better performance at low TSRs. A two-dimensional computational analysis was conducted and two-equation Shear Stress Transport (SST) turbulence model was employed to close the RANS equations. The obtained results indicated that the performance of the VAWT can be improved by using J-shaped profiles for the blade sections.

Another study which focused on increasing the performance of VAWTs was done by Nobile *et al.* (2014). In their research, a 2D computational simulation of an augmented wind turbine was carried out. The influence of mesh resolution, turbulence model, and time step on results accuracy was investigated. It was concluded that the mesh resolution and the turbulence model affect the results accuracy, while the time step size has small impact on numerical results. The numerical simulation results showed that the introduction of an omnidirectional stator around the wind turbine rotor increases the power and torque coefficients by around 30–35%. Mohamed (2012) performed a comparison between ANSYS Workbench and Gambit meshing tools. Following that comparison, unsteady simulations were performed for different speed ratios based on URANS turbulence models using sliding mesh approach. The results showed that the accuracy of simulations which used ANSYS Workbench meshing is improved by using SST K-ω model. In addition, the turbine performance was compared using different airfoil profiles and the results showed that new airfoils can increase efficiency by 10% compared with regular airfoils.

One of the most important aspects in VAWT simulations is the proper modeling of turbulence. A systematic numerical analysis was done by Daróczy *et al*. (2015) to identify the necessary mesh resolution for different turbulence models. The URANS-based 2D computations of H-Darrieus wind turbines were conducted and compared. The results showed that the k-ε Realizable model is able to predict Cp with an almost constant offset compared to the experimental data. The k-ω SST model with a cubic correction delivered an excellent prediction for three out of forth rotor configurations. Chowdhury *et al*. (2016) performed a numerical simulation of a vertical axis wind turbine in upright and tilted conditions. Three turbulence models of RNG k-ε, Spalart-Allmaras, and SST k-ω were used in the research. It was demonstrated that Spalarte-Allmaras model is not compatible with the simulation objectives. SST k- ω is seen to capture the wake vortices better than RNG k-ε. Also, the result obtained from SST k-ω was the closest to the experimental values.

Marsh *et al.* (2017) investigated the power output of two fixed pitch vertical axis turbines using 2D and 3D CFD models with different turbulence and boundary layer flow modeling techniques. It was demonstrated that although the k-ω SST Transition model is in the highest correlation with experimental power output data, the fully turbulent 3D k-ω SST model is better suited for vertical axis turbine simulation. Balduzzi *et al*. (2016) performed an extended analysis with the aim of identifying the most effective simulation settings to ensure a reliable unsteady, two-dimensional simulation of an H-type Darrieus turbine. The results showed that the k-ω SST turbulence model is the most suitable choice for the simulation of Darrieus turbines. It was resulted that a properly adjusted two-dimensional approach is definitely able to describe the actual functioning of Darrieus rotors.

Rolland *et al.* (2013) developed a CFD based computational model which provided a useful tool for the assessment of designs for VAWTs. The CFD model reflected the experimental data well. The numerical values were in good agreement with overall power output and pressure distribution. Considerable deviations from the experimental results were observed when extreme values of geometrical angle were used. These deviations were attributed to the simplified turbulence modelling approach. Furthermore, Aresti *et al.* (2013) presented a numerical approach to predict the performance of vertical axis wind turbines based on moving mesh technique. The turbulence was modeled using Renormalization Group (RNG) $k-\varepsilon$, standard $k-\varepsilon$ and $k-\omega$ turbulence models. Two dimensional and three-dimensional simulations were carried out and the simulation predictions were used to determine the performance of the turbine. The results of the study showed that self-starting capabilities of the turbine can be increased when the mounted angle of attack of the blades is increased.

Ferrari *et al.* (2017) conducted a CFD study to characterize the dynamic behavior of a Savonius vertical axis wind turbine using the open source code, OpenFOAM. Unsteady simulations were carried out at different tip speed ratios, various angular speeds of rotor at constant wind speed, and different URANS turbulence models. The results of 3D model were in good agreement with experiments, while 2D model is characterized by higher lift than the full three-dimensional simulation.

A brief review of the literature implies that CFD is a promising tool to study the effects of various parameters on vertical axis wind turbine performance. Investigating the effect of turbulence models, especially the transition models on results accuracy is an open field to study. In this paper, numerical optimization of a VAWT based on a transition turbulence model has been carried out to propose an alternative source of energy for tall buildings. Based on the proposed numerical model, a case study was conducted to consider the installation of four VAWTs in the southwest corner of medical science building at TMU campus.

2. Governing equations

By passing through the rotor of a turbine, wind's kinetic energy is absorbed by the rotor and wind speed is reduced. This means a reduction in flow momentum from upstream to downstream. This change in momentum can be attributed to a force resulted from pressure change in two sides of the rotor. By setting the change in momentum equal to the force

resulted from change in pressure, the maximum power coefficient which is called the Betz limit can be calculated (Mathew 2006). The Betz limit is the maximum theoretical value of power coefficient and lower peak values are achievable in practice. The power coefficient of a rotor varies with tip speed ratio (Eq. (1)) and it is only maximum for a unique tip speed ratio (Righter 1996).

$$\lambda = \frac{R\omega}{V_\infty} \tag{1}$$

2.1 Reynolds-Averaged Navier-Stokes (RANS)

Governing equations of fluid flow are time-averaged continuity in accordance with the time-averaged momentum equations (Durbin and Reif 2011). Since the effect of heat loss is considered negligible, there's no need to solve the energy equation. In addition, because of the little effect of gravity on fluid field, the gravity term is disregarded. Considering a negligible variation in flow field parameters in direction of (z), continuity and momentum equations were solved in 2D. The governing equations are shown as follows.

$$\frac{\partial \bar{u}_i}{\partial x_i} = 0 \tag{2}$$

$$\frac{\partial \bar{u}_i}{\partial t} + \bar{u}_j \frac{\partial \bar{u}_i}{\partial x_j} = \frac{1}{\rho}\frac{\partial}{\partial x_j}(\tau_{ij}^{eff}) \tag{3}$$

$$\tau_{ij}^{eff} = -\bar{p}\delta_{ij} + \mu\left(\frac{\partial \bar{u}_i}{\partial x_j} + \frac{\partial \bar{u}_j}{\partial x_i}\right) - \rho\overline{u'_i u'_j} \tag{4}$$

The last term in Eq. (4) is Reynolds stress term. This term is modeled by a turbulence model. A common method employs the Boussinesq hypothesis to relate the Reynolds stresses to the mean velocity (Fluent 2013).

$$-\rho\overline{u_i u_j} = \mu_t\left[\frac{\partial \bar{u}_i}{\partial x_j} + \frac{\partial \bar{u}_j}{\partial x_i}\right] - \frac{2}{3}\delta_{ij}\left[\rho k + \mu_t \frac{\partial \bar{u}_k}{\partial x_k}\right] \tag{5}$$

The Boussinesq hypothesis is used in Spalart-Allmaras model, $k-\varepsilon$ models, and $k-\omega$ models. Regarding the Reynolds number on blades and the physics of the turbulent flow, the two equation shear-stress transport (SST) $k-\omega$ and the SST-Transition model were used in this research.

2.2 SST $k-\omega$ turbulence Model

The shear-stress transport SST $k-\omega$ model was developed by Menter (1994) to combine the accurate formulation of the $k-\omega$ model in vicinity of the wall region with the freestream independence of the $k-\varepsilon$ model in the far field. The SST $k-\omega$ model is similar to the standard $k-\omega$ model including some modifications. These modifications make the SST $k-\omega$ model more accurate and reliable than the standard $k-\omega$ model for a wide variety of engineering applications including adverse pressure gradient flows and airfoil flows.

The turbulence model is based on two transport equations for the turbulence kinetic energy k and the specific dissipation rate ω which is equal to the ratio of ε to k.

The turbulence kinetic energy and the specific dissipation rate are defined by the Eqs. (6) and (7) (Fluent 2013). In the these equations, the term G_k represents the production of turbulence kinetic energy due to mean velocity gradients and G_ω represents the generation of ω. Γ_k and Γ_ω represent the effective diffusivity of k and ω respectively. Moreover, Y_k and Y_ω represent the dissipation of k and ω due to turbulence. Finally, D_ω stands for the cross diffusion term while S_k and S_ω are user-defined source terms (Fluent 2013).

2.3 Transition SST turbulence model

The most problematic issue in CFD simulation of an airfoil at low Reynolds number is to capture the stall phenomena. This is due to the inefficiency of RANS turbulence models to accurately capture the boundary layer separation caused by adverse pressure gradient. Moreover, at low Re, a fairly large portion of the boundary layer is laminar, thus a fully turbulent model cannot predict the boundary layer behavior precisely. As the accurate modeling of the boundary layer is of great importance for simulating VAWTs, utilizing a transition model can result in a more realistic prediction of turbine performance (Lanzafame *et al.* 2014).

Transition occurs through different mechanisms. Primary modes of transition are often referred to as natural, bypass and separated flow transition. Natural transition is typically the result of flow instability (Tollmien-Schlichting waves or cross-flow instability), where the resulting

$$\frac{\partial}{\partial t}(\rho k) + \frac{\partial}{\partial x_i}(\rho k u_i) = \frac{\partial}{\partial x_j}\left(\Gamma_k \frac{\partial k}{\partial x_j}\right) + G_k - Y_k + S_k \tag{6}$$

$$\frac{\partial}{\partial t}(\rho \omega) + \frac{\partial}{\partial x_j}(\rho \omega u_j) = \frac{\partial}{\partial x_j}\left(\Gamma_\omega \frac{\partial \omega}{\partial x_j}\right) + G_\omega - Y_\omega + D_\omega + S_\omega \tag{7}$$

$$\frac{\partial(\rho\gamma)}{\partial t} + \frac{\partial\left(rU_j\gamma\right)}{\partial x_j} = P_{\gamma 1} - E_{\gamma 1} + P_{\gamma 2} - E_{\gamma 2} + \frac{\partial}{\partial x_j}\left[\left(\mu + \frac{\mu_t}{\sigma_\gamma}\right)\frac{\partial \gamma}{\partial x_j}\right] \tag{8}$$

$$\frac{\partial\left(\tilde{\mathrm{Re}}_{\theta t}\right)}{\partial t} + \frac{\partial\left(\rho U_j \tilde{\mathrm{Re}}_{\theta t}\right)}{\partial x_j} = P_{\theta t} + \frac{\partial}{\partial x_j}\left[\sigma_{\theta t}\left(\mu + \mu_t\right)\frac{\partial \tilde{\mathrm{Re}}_{\theta t}}{\partial x_j}\right] \tag{9}$$

$$\frac{\partial}{\partial t}(\rho k) + \frac{\partial}{\partial x_i}(\rho k u_i) = \frac{\partial}{\partial x_j}\left(\Gamma_k \frac{\partial k}{\partial x_j}\right) + G_k^* - Y_k^* + S_k^* \tag{10}$$

$$G_k^* = \gamma_{eff} \tilde{G}_k$$

$$Y_k^* = \min\left(\max\left(\gamma_{eff}, 0.1\right), 1.0\right) Y_k^*$$

exponential growth of two-dimensional waves eventually results in a non-linear break-down to turbulence. Bypass transition is imposed on the boundary layer by high levels of turbulence in the freestream. For transition at high freestream turbulence levels (>1%), the first stages of the natural transition process may be bypassed such that turbulent spots are directly produced within the boundary layer by the influence of freestream disturbances. Finally in separation-induced transition, laminar boundary layer separates under the influence of a pressure gradient and transition develops within the separated shear layer (Langtry 2006).

Although significant progress has been made in the development and implementation of turbulence models, the important effect of laminar-turbulent transition is rarely included in the majority of CFD simulations. In the present research a laminar to turbulent transition model is used to simulate the flow in order to increase the accuracy of the simulation. The transition model formulation is based on two transport equations. These transport equations do not attempt to model the physics of the transition process, but form a framework for the implementation of correlation-based models into CFD method. The physics of the transition process are contained entirely in empirical correlations (Menter *et al.* 2006).

The transition SST model is based on the combination of SST $k-\omega$ transport equations with two other transport equations, one for the intermittency and another for the transition onset criteria, in terms of Reynolds number based on momentum-thickness (Menter *et al*. 2003). The transport equation for the intermittency γ is defined as Eq. (8) (Fluent 2013).

In Eq. (8), $P_{\gamma 1}$ and $P_{\gamma 2}$ are transition source terms whereas $E_{\gamma 1}$ and $E_{\gamma 2}$ are destruction/relaminarization sources (Menter *et al*. 2006).

The transport equation for the transition Reynolds number $\tilde{\mathrm{Re}}_{\theta t}$ is shown in Eq. (9). The detailed description on calculation methods for the source terms in Eqs. (8) and (9) as well as the three empirical correlations of the model used for calculating the transition onset, the length of the transition zone and the point where the model is activated is discussed thoroughly by Menter *et al*. (2006).

The transition model interacts with the SST turbulence model by modification of the k equation as shown in Eq. (10).

In Eq. (10), G_k^* and Y_k^* are the original production and destruction terms for the SST model. In order to capture the laminar and transitional boundary layers correctly, the mesh must have a y^+ of approximately one.

In above equations, G_k^* and Y_k^* are the original production and destruction terms for the SST model. In order to capture the laminar and transitional boundary layers correctly, the mesh must have a y^+ of approximately one.

3. Turbine specification, simulation domain and grid generation

In this study, to evaluate the employed transition turbulence model, and to validate the proposed numerical model, Howell experimental data was used (Lanzafame *et al.* 2014). The specifications of Howell turbine are presented in Table 1 and the 2D simulation field is specified as a 35 m × 7.5 m rectangle as show in Fig. 1.

As it is shown in Fig. 1, the effect of wind turbine struts and rotor shaft is ignored as it is not possible to consider these components in 2D simulation.

The elimination of struts has little effect on the wake flow of vertical axis wind turbines and the main contribution for the flow around this type of turbine is made by turbine blades (Mendoza *et al.* 2018). For this particular turbine considered in this study (3-bladed wind turbine with solidity of about 0.16) the 2D simulations would lead to acceptable results (Delafin *et al*. 2016). Boundary conditions of the flow field are demonstrated in Table 2.

Because of the importance of flow in vicinity of the blades, an inflation layer (boundary layer) mesh was used on airfoils as shown in Fig. 2.

Table 1 Specifications of the studied turbine (Lanzafame *et al.* 2014)

Characteristic	Value
Number of blades	3 Pcs
Blade chord length	0.4 m
Blade section airfoil	NACA 0015
Wind speed	6-12 m/s
Initial Step	0 degrees
Rotor radius	1.25 m
Blade height	1 m
Arm diameter	20 mm
Number of arms	6 Pcs

Table 2 Boundary conditions of the simulation domain

Boundary	Value
Inlet velocity	10 m/s
Rotor rotational speed	120 rpm
Air density	1.22 kg/m^3
Fluid pressure	1 atm
Inlet boundary condition	Velocity inlet
Outlet boundary condition	Pressure outlet
Side walls boundary condition	Symmetry

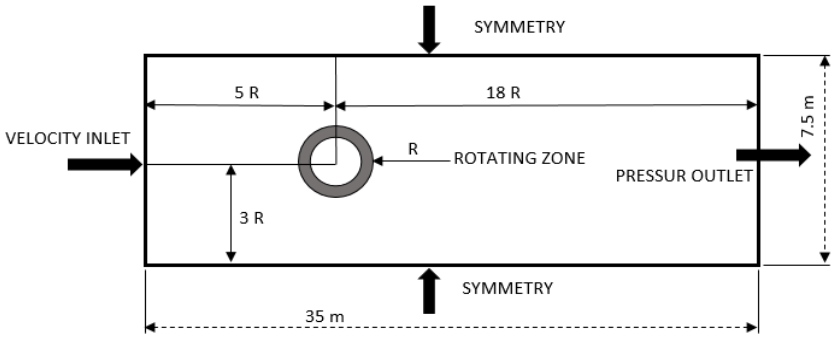

Fig. 1 Geometrical features and main dimensions of the computational domain

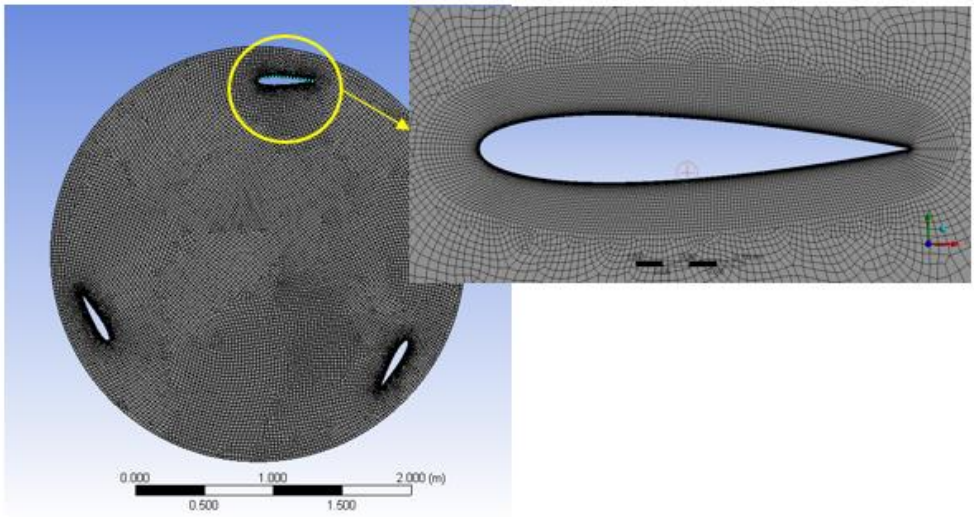

Fig. 2 Scheme of mesh distribution in rotating zone area (left), inflation layer on the airfoils (right)

Total rotor generated torque is oscillating in nature. Therefore, average torque value should be used to calculate turbine power coefficient which is shown in Eq. (11). The torque coefficient is calculated by Eq. (12) (Burton *et al.* 2012, Lanzafame *et al.* 2014).

$$C_p = \frac{\overline{T}.\omega}{0.5\rho DHV_\infty^3} \tag{11}$$

$$C_m = \frac{\overline{T}}{0.5\rho V_\infty^2 DHR} \tag{12}$$

4. Investigating the grid and time step independency

Fig. 3 demonstrates the power coefficient for 6 grids with different number of nodes. The number of nodes on airfoil surface as well as the number of inflation layers was gradually increased to obtain grid independency. The figure shows that increasing the number of cells from 800,000 to 1,200,000 has little effect on results. Therefore, based on the results showed in Fig. 3, the grid with 800,000 nods was chosen as the suitable grid for simulations.

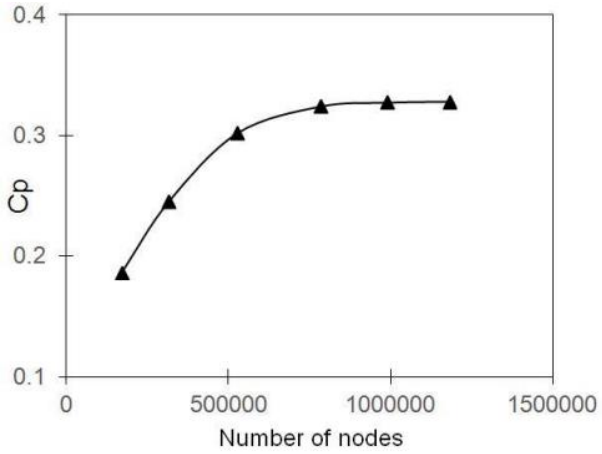

Fig. 3 Power coefficient vs. number of nodes to ensure grid independency

To investigate the effect of time step value on results, two simulations were performed using time steps corresponding to 0.5 and 1 degrees of rotor rotation. The maximum of 4.5% difference in power coefficient value was observed. Consequently, the time step corresponding to 1-degree rotation of rotor was chosen to solve the problem.

Number of rotor rotations required to achieve a developed generated torque coefficient in tip speed ratio of 1.5 is demonstrated in Fig. 4. According to Fig. 4, the results were studied from 6th rotation onward (Mohamed 2012).

The most important parameters in wind turbine performance are the turbine generated power and torque. These parameters are used to study the effects of different factors on wind turbine performance. The generated power in a real turbine is the amount of power received from turbine generator. In numerical simulation, power is calculated from shaft torque multiplied by turbine angular speed; though the amount of power calculated through this method neglects the loss from friction specially in the turbine gearbox and the effect of generator efficiency. Normally, the wind turbine generator and gearbox have a combined efficiency of 90%. Therefore, to investigate real turbine efficiency, the calculated power resulted from multiplying shaft torque by angular speed, should be corrected by applying a 0.9 correction factor (Burton *et al.* 2012).

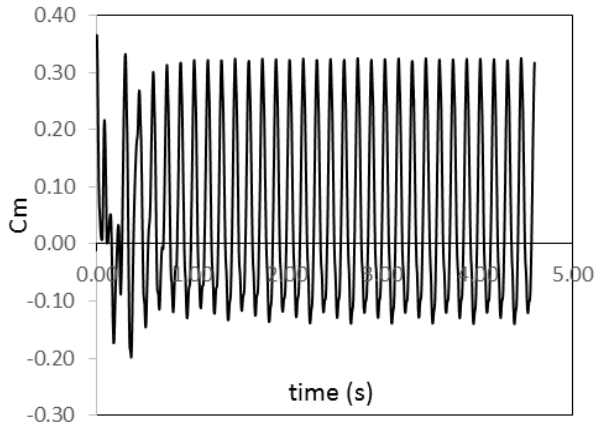

Fig. 4 Torque coefficient vs. time to determine the number of rotor rotations required to achieve a developed generated torque

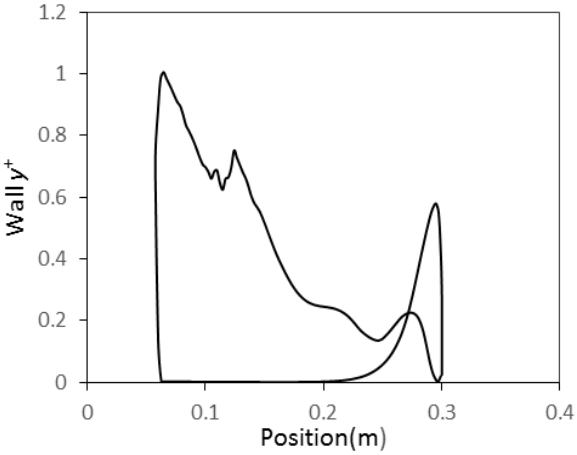

Fig. 5 y^+ on turbine blade surface

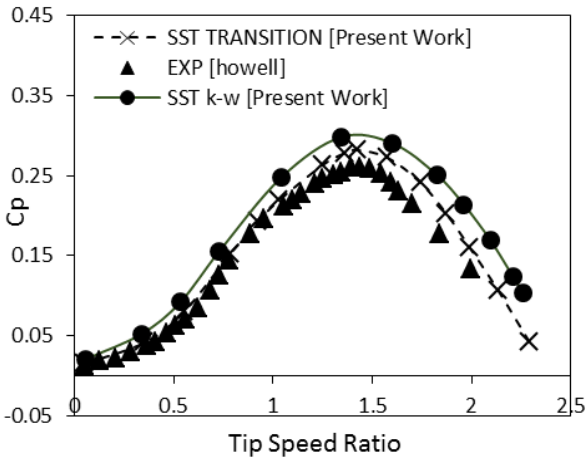

Fig. 6 Power coefficient curve vs. TSR for utilized turbulence models as well as experimental data

One of the important and effective factors in numerical simulation accuracy, is the amount of y^+ (Fluent 2014). Fig. 5 shows the y^+ value on blade wall based on 120 rpm rotary speed. According to Fig. 5, the magnitude of y^+ is below 1 on blade wall, consequently, the grid size is considered to be suitable to accurately capture the boundary layer on blade surface.

5. Validating the simulation results

After conducting the grid and time step independency and investigating sufficient number of rotations, turbine power coefficient vs. λ using the two SST-Transition and SST k-ω turbulence models is demonstrated. The resulted turbine power coefficient is compared to the experimental results presented by Howell *et al.* (2010). The results are shown in Fig. 6.

Table 3 shows the mean error between simulation results and experimental data.

Table 3 Turbulence model power coefficient mean error absolute value

Blade tip speed	Error (%) SST k-ω	Error (%) SST- Transition
0.5	8.2	1.7
0.8	9.03	5.05
1	14.2	4.9
1.25	15.5	6.9
1.5	15.6	7.6
1.75	18.93	11.05
2	19.21	12.3
Mean Error	15.51	7.84

It can be seen that both turbulence models over-predicted the power coefficient. It is because of employing 2D method and ignoring 3D effects like the effects of turbine struts. Moreover, the effect of tip loses which is present in experiments cannot be captured in 2D simulations. The deviation between experimental and simulation results increases as the tip speed ratio grows. This deviation can be attributed to inherent 3D flow complexities which are not taken into account in 2D simulation (Rezaeiha *et al.* 2017). Capturing stall phenomenon is challenging when RANS equations are being used for turbulence modeling. Vertical axis wind turbine blades experience laminar, transient, and turbulent regimes during each cycle of rotation and an important portion of boundary layer is laminar specially in low Re numbers. Therefore, the use of classical fully turbulent model is not accurate enough. This is the reason for more realistic predictions of transition model demonstrated in Fig. 6. Based on the above discussion and the results presented in Table 3, SST-Transition model is used to perform simulations.

By passing the stream over the rotor blades, vertical and tangential forces are exerted to the blade's center of pressure, consequently, generated torque is a result of these two components. Reference blade generated torque curve in one rotor rotation at 10 m/s wind speed can be seen in Fig. 7. Fig. 8 demonstrates the torque coefficient of 3 blades in 360-degrees rotation separately as well as the total torque value resulted from the summation of all 3 blades. As showed in Fig. 7, the wind energy is absorbed by the blade in rotor upstream section. Only a small part of stream energy is transferred to the rotor blade downstream.

It's important to note that, in downstream region, sometimes the generated torque is in the opposite direction of the rotation, which reduces the overall performance of the rotor (Biadgo *et al.* 2013).

In each angle, total rotor generated torque is the summation of the torque value generated by each blade in Fig. 8. In is clear that the total rotor generated torque is oscillating so the average torque value is used to calculate the turbine power coefficient.

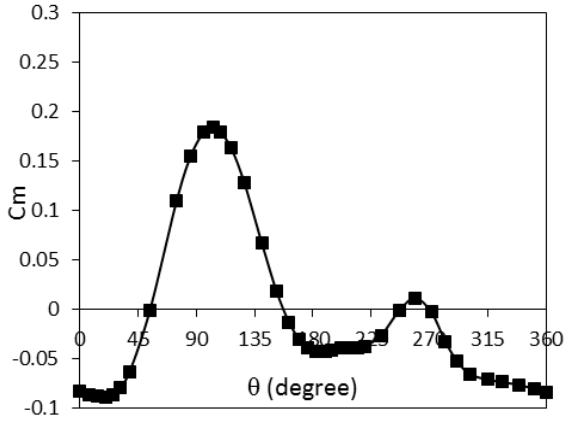

Fig. 7 One blade torque coefficient in 360-degrees rotation

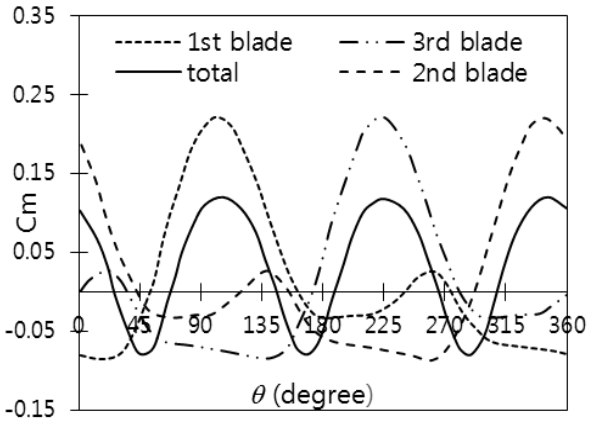

Fig. 8 Torque coefficient of 3 blades in 360-degrees rotation and total torque of the rotor

6. Parametric study and numerical optimization

In this section, the effect of two Influential factors on turbine performance will be investigated.

6.1 Investigation of the effects of shaft arm connection position to the blade

To study the effects of changing the blade connection position on turbine performance, 4 rotors with different connection positions are considered as shown in Fig. 9. In the figure, the first spot is in aerodynamic center, the second one is in maximum thickness, the third spot is in surface center and the fourth is located in the middle of airfoil chord.

Fig. 10 shows the power coefficient curve for the four connection spots defined in Table 4 in various blade tip speed ratios.

From the results demonstrated in Fig. 10 it can be deducted that increasing the arm connection distance from blade leading edge, up to 0.4 m will result in power increase. However, increasing the distance further causes the power to be reduced. Power coefficient increase could be attributed to the increased torque resulted from vertical forces. In 0.25 and 0.3 distances, pressure center is situated between the connection spot and the blade trailing edge, and in the angles where force is applied in the positive direction, pressure center is moved to the distance between leading edge and connection spot. This in whole results in the generated torque to be opposite to rotor rotational direction.

Table 4 Rotor arm connection spot to the blade

Rotor	Connection spot (meters)
Rotor 1	C=0.25m
Rotor 2	C= 0.30m
Rotor 3	C=0.4 m
Rotor 4	C=0.5 m

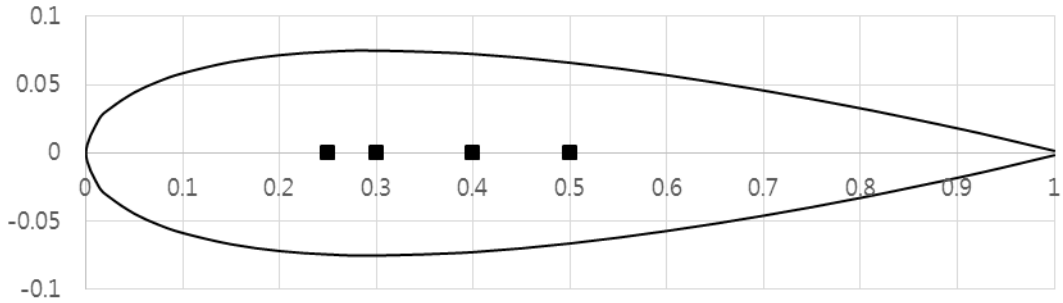

Fig. 9 Arm connection positions

For the connection spots in 0.4 and 0.5, the pressure center is always between the blade leading edge and the connection spot. This causes the emergent generated torque in the angles where the vertical force is in negative direction to be applied in the rotor rotational direction and create a positive torque (Hameed and Afaq 2013).

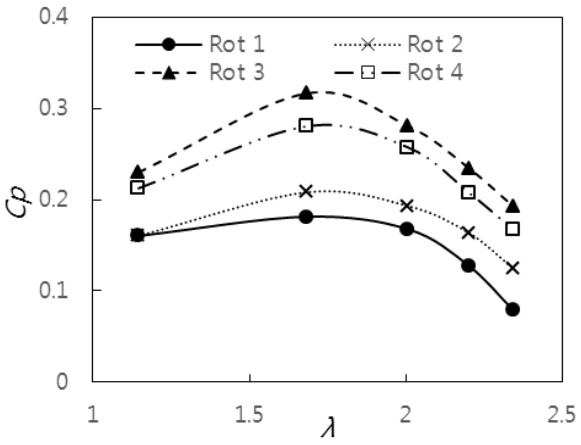

Fig. 10 Power coefficient curve vs. tip speed ratio for different blade arm connection spots

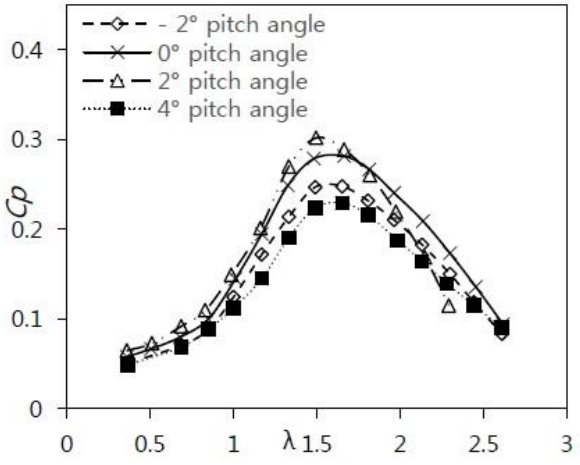

Fig. 11 Variation in power coefficient curve vs. tip speed ratio for different pitch angles

6.2 Investigating the change in blade pitch angle

Another important influential factor on turbine aerodynamics, is the blade pitch angle. To assess the effects of this factor, blade pitch angles between -2° and 4° at wind speed of 10 m/s and angular speed of 120 rpm were considered. The results are shown in Fig. 11.

The results of Fig. 11 show that for a specific tip speed, power coefficient increases the most from pitch angle of -2° to pitch angle of 2°, and by further increasing the angle to 4°, the power coefficient is reduced. This is due to the increase of the lift force on blades for the former case and decrease of the force on later.

7. Case study: simulation of VAWTs on TMU medical science building

According to the results of a recent research (Jadidi and Heidarinejad 2015) which simulated the turbulent wind flow on TMU buildings using DES and LES turbulence models, the fastest western wind blows to the southwest corner of medical science building. As a case study, a vertical axis wind turbine was simulated in the southwest corner of the medical science building (Fig. 12) at 50°48’ longitude and 35°72’ latitude, at the height of 42 meters from the ground and 1314 meters from sea-level (Shamsi 2010).

In order to determine the location and position of the wind turbine in vicinity of the building, the wind flow around the south side of the medical science building was simulated two-dimensionally. The result shows the maximum speed is achievable in A, B, C and D points in Fig. 12.

The speed profile for solving the boundary layer problem is shown in Eq. (13) (Jadidi and Heidarinejad 2015). In this equation, υ is wind velocity and z is the height.

$$\frac{v_2}{v_1} = \left(\frac{z_2}{z_1}\right)^{0.3} \tag{13}$$

According to the reports and statistics, the wind speed used in simulations is chosen 5.6 m/s at the height of 10 meters from the ground (Keyhani *et al.* 2010). Eq. (17) was then used to calculate wind speed at heights between 10 to 42 meters.

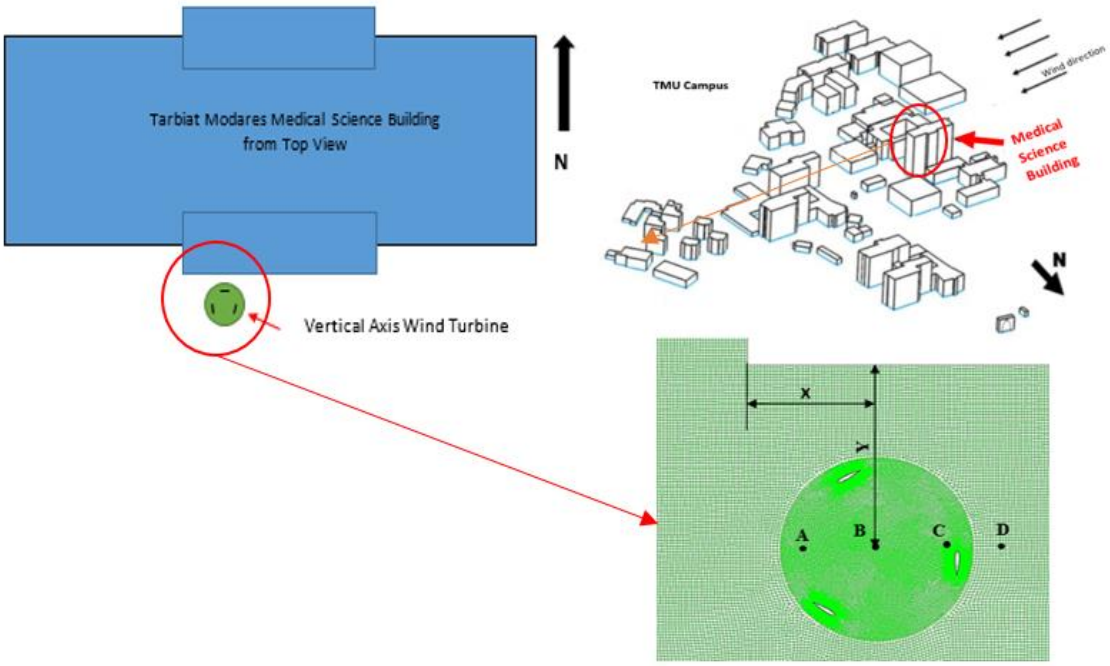

Fig. 12 Top view of Tarbiat Modares Medical Science Building and the turbine position (Jadidi and Heidarinejad 2015)

According to the dimensions of the medical science building, the specifications of the turbine, and the area of the highest speed at turbine upstream, the installation position of the turbine was chosen on the line of Y=1.25 m. To determine the best position, the achievable power was calculated for the four selected spots of A, B, C, D as showed in Fig. 12. The coordinates of the selected points are shown it Table 5.

The power coefficient in the four A, B, C, D spots is shown in Fig. 13. Regarding the wind speed profile and the curves of Fig. 13, we realize that point C generates the maximum power coefficient among the 4 points mentioned above. Therefore, the installation location is chosen to be at point C, at heights 30 to 42 meters in which four vertical axis turbines can be installed.

Turbine generated power versus wind speed in point C can been seen in Fig. 14. Based on Eq. (14), turbine power increases by increasing free stream speed. This may increase the forces beyond limit and as a result, damage the turbine. Usually the turbines are equipped with a control system designed to prevent increasing rotor rotation speed.

Table 5 Rotor position according to Fig. 12

position	X (m)	Y (m)	Z (m)
Position A	1	2.25	30
Position B	1.5	2.25	30
Position C	2	2.25	30
Position D	2.5	2.25	30

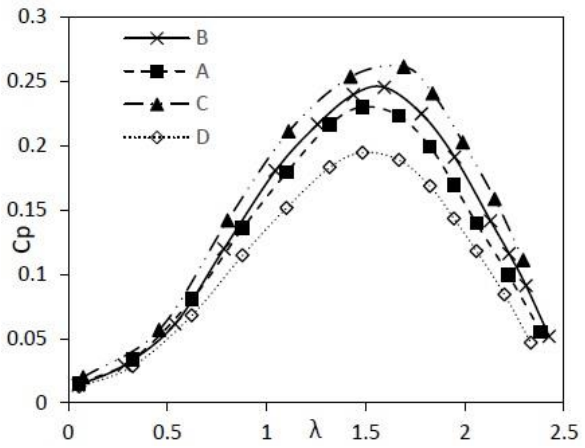

Fig. 13 Power coefficient curve in four points of A, B, C, and D in the vicinity of the building

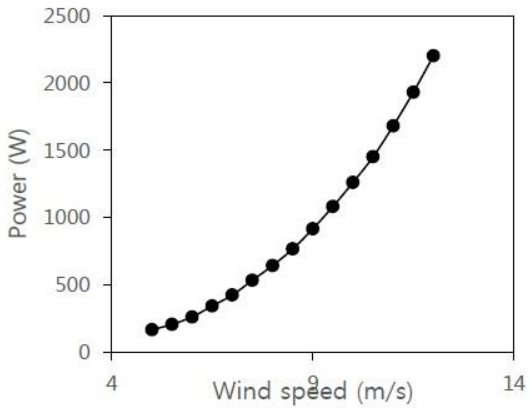

Fig. 14 Turbine generated power vs. wind speed in point C location

Thus, the power diagram is considered to be constant in accordance with the maximum wind speed of 12 m/s (Lanzafame *et al.* 2014).

$$P = 0.5 \times C_p \times \rho_{air} \times v^3 \times A \times H_S \quad (14)$$

Due to the variation of wind speed and subsequently turbine generated power, field studies were conducted using Meteorology Organization statistics and the processed data using commercial wind analysis software, WindPro. Turbine generated power as a function of region wind speed was calculated by Eq. (15). By having power as a function of speed and using region statistics, the generated power per year can be calculated by Eq. (16) (IRIMO 2008).

$$f(v) = \frac{k}{c}\left(\frac{v}{c}\right)^{k-1} exp\left(-\frac{v}{c}\right)^{k} \quad (15)$$

$$\bar{P}_{total} = (\int_0^{\infty} f(v)\, power(v) dv) N \Delta t \quad (16)$$

In Eq. (16), N equals 52560 which is the number of data in a year. Δt is equal to 10 minutes. By solving the equation and using the wind distribution function, the amount of yearly generated power by four 1.5 KW turbines stationed at 30 to 42-meters height on TMU medical science building can be calculated. The magnitude of yearly generated power according to Eq. (17) is equal to 8.28 MWh.

$$\sum_{p=1}^{4} \bar{P}_{total} = 8.287 MWh \quad (17)$$

8. Conclusions

In this study, an aerodynamic numerical simulation of a vertical axis wind turbine was conducted. The data from several experiments conducted on a real 0.5 kW capacity turbine found in literature were used to evaluate the simulation results. The power coefficient values resulted from aerodynamic simulations using two SST k-ω and SST-Transition turbulence models were studied and compared. Because of the conformity of the results to those of experiments, SST-Transition turbulence model was chosen as the proper model for simulations. It was also found that the accuracy of numerical simulation is highly dependent on the quality of the grid around the blades. Two aerodynamic factors affecting turbine performance were investigated. It was concluded that in a specific tip speed ratio, turbine power coefficient is maximum at 2° pitch angle. The other investigated parameter was the effect of turbine shaft connection arm position. It was shown that at C=0.4 m the amount of power coefficient is at its maximum. As a case study, four vertical axis turbines at the height of 30 to 42 meters on the south side of TMU medical science building were simulated. Considering the local wind speed profile, at 42-meter height, the turbine power peaks at 2.32 MWh and at 30 meters, the power reached its lowest point at 1.86 MWh**.** The annual total generated power of 8.28 MWh was obtained based on calculations.

References

Aresti, L., Tutar, M., Chen, Y. and Calay, R.K. (2013), "Computational study of a small scale vertical axis wind turbine (VAWT): comparative performance of various turbulence models", *Wind Struct.*, **17**(6),647-670

Balduzzi, F., Bianchini, A., Maleci, R., Ferrara, D. and Ferrari, L. (2016), "Critical issues in the CFD simulation of Darrieus wind turbines", *Renew. Energ*., **85**, 419-435

Biadgo, M.A., Simonović, A., Komarov, D. and Stupar, S. (2013), "Numerical and analytical investigation of vertical axis wind turbine", *FME Transactions*, **41**(1), 49-58

Burton, T., Sharpe, D., Jenkins, n. and Bossanyi, E. (2012), Wind Energy Handbook, John Wiley & Sons.

Chowdhury, A.M., Akimoto, H. and Hara, Y. (2016), "Comparative CFD analysis of Vertical Axis Wind Turbine in upright and tilted configuration", *Renew. Energ*., **85**, 327-337

Cooney, C., Byrne, R., Lyons, W. and O'Rourke, F. (2017), "Performance characterisation of a commercial-scale wind turbine operating in an urban environment, using real data", *Energy for Sustainable Development*, **36**, 44-54

Daróczy, L., Janiga, G., Petrasch, K., Webner, M. and Thévenin., D. (2015), "Comparative analysis of turbulence models for the aerodynamic simulation of H-Darrieus rotors", *Energy*, **90**(1), 680-690

Delafin, P.L., Nishino, T.., Wang, L. and Kolios, A. (2016), "Effect of the number of blades and solidity on the performance of a vertical axis wind turbine", *J. Phys.: Conference Series*, **753**(2), 022033

Dobrev, I. and Massouh, F. (2011), "CFD and PIV investigation of unsteady flow through Savonius wind turbine", *Energy Procedia*, **6**, 711-720

Durbin, P.A. and Reif, B A.P. (2011), Statistical Theory and Modeling for Turbulent Flows, John Wiley & Sons.

Ferrari, G., Federici, D., Schito, P., Inzoli, F. and Mereu, R. (2017), "CFD study of Savonius wind turbine: 3D model validation and parametric analysis", *Renew. Energ*., **105**, 722-734

Fluent, ANSYS (2013), ANSYS fluent theory guide 15.0.

Fluent, ANSYS (2014), ANSYS fluent theory guide 16.0.

Hameed, M.S. and Afaq, S.K. (2013), "Design and analysis of a straight bladed vertical axis wind turbine blade using analytical and numerical techniques", *Ocean Eng*., **57**, 248-255

Howell, R., Qin, N., Edwards, J. and Durrani, N. (2010), "Wind tunnel and numerical study of a small vertical axis wind turbine", *Renew. Energ*., **35**(2),412-422

IRIMO (2008), National Centre of Climatology Report. Islamic Republic of Iran Meteorological Organization.

Islam, Mazharul, David S. K. Ting, and Amir Fartaj. (2008) "Aerodynamic models for Darrieus-type straight-bladed vertical axis wind turbines", *Renew. Sust. Energ. Rev*., **12**(4),1087-1109

Jadidi, A.M. and Heidarinejad, G. (2015), "Turbulent wind flow simulation over Tarbiat Modares University", *Mod. Mech. Eng*., **14** (13), 272-280.

Keyhani, A., Ghasemi-Varnamkhasti, M., Khanali, M. and Abbaszadeh, R. (2010), "An assessment of wind energy potential as a power generation source in the capital of Iran, Tehran", *Energy*, **35**(1), 188-201

Langtry, R.B. (2006), "A correlation-based transition model using local variables for unstructured parallelized CFD codes", Ph.D. Dissertation, Mechanical Engineering, University of Stuttgart, Stuttgart, Germany

Lanzafame, R., Mauro, S. and Messina, M. (2014), "2D CFD modeling of H-Darrieus wind turbines using a transition turbulence model", *Energy Procedia*, **45**, 131-140

Lee, Y.T. and Lim, H.C. (2015), "Numerical study of the aerodynamic performance of a 500 W Darrieus-type vertical-axis wind turbine", *Renew. Energ.*, **83**,407-415

Lin, S.Y., Lin, Y.Y., Bai, C.J. and Wang, W.C. (2016), "Performance analysis of vertical-axis-wind-turbine blade with modified trailing edge through computational fluid dynamics", *Renew. Energ.*, **99**, 654-662

Marini, M., Massardo, A. and Satta, A. (1992), "Performance of vertical axis wind turbines with different shapes", *J. Wind Eng. Ind. Aerod.*, **39**(1-3), 83-93

Marsh, P., Ranmuthugala, D., Penesis, I. and Thomas, G. (2017), "The influence of turbulence model and two and three-dimensional domain selection on the simulated performance characteristics of vertical axis tidal turbines", *Renew. Energ.*, **105**, 106-116

Mathew, S. (2006), Wind energy fundamentals,resource analysis and economics, second ed. Vol. 1. Berlin, Springer Science & Business Media

McTavish, S., Feszty, D. and Sankar, T. (2012), "Steady and rotating computational fluid dynamics simulations of a novel vertical axis wind turbine for small-scale power generation", *Renew. Energ.*, **41**, 171-179

Mendoza, V., Bachant, P., Ferreira, C. and Goude, A. (2018), "Near-wake flow simulation of a vertical axis turbine using an actuator line model", Wind Energy

Menter, F.R. (1994), "Two-equation eddy-viscosity turbulence models for engineering applications", *AIAA J.*, **32**(8), 1598-1605

Menter, F.R., Kuntz, M. and Langtry, R. (2003), "Ten years of industrial experience with the SST turbulence model", *Turbul. Heat Mass Transfer*, **4**(1), 625-632

Menter, F.R., Langtry, R. and Völker, S. (2006), "Transition modelling for general purpose CFD codes", Flow Turbul. Combust., **77**(1), 277-303

Menter, F.R., Langtry, R.B., Likki, S.R., Suzen, Y.B., Huang, P.G. and Völker, S. (2006), "A correlation-based transition model using local variables—Part I: model formulation", *J. Turbomachinery*, **128**(3), 413-422

Mohamed, M.H. (2012), "Performance investigation of H-rotor Darrieus turbine with new airfoil shapes", *Energy*, 47(1), 522-530

Nobile, R., Vahdati, M., Barlow, J.F. and Mewburn-Crook, A. (2014), "Unsteady flow simulation of a vertical axis augmented wind turbine: A two-dimensional study", *J. Wind Eng. Ind. Aerod.*, **125**, 168-179

Rezaeiha, A., Kalkman, I. and Blocken, B. (2017), "Effect of pitch angle on power performance and aerodynamics of a vertical axis wind turbine", *Appl. Energ.*, **197**, 132-150

Righter, R.W. (1996), Wind Energy in America: A history, University of Oklahoma Press.

Rolland, S., Newton, W., Williams, A.J., Croft, T.N., Gethin, D.T. and Cross, M. (2013), "Simulations technique for the design of a vertical axis wind turbine device with experimental validation", *Appl. Energ.*, **111**,1195-1203

Shamsi, R. (2010), Tehran Yearly Wind Statistic. Tehran.

Soto, A.M. and Jentsch, M.F. (2016), "Comparison of prediction models for determining energy demand in the residential sector of a country", *Energ. Build.*, **128**,38-55

Zamani, M., Maghrebi, M.J. and Moshizi, S.A. (2016), "Numerical study of airfoil thickness effects on the performance of J-shaped straight blade vertical axis wind turbine", *Wind Struct.*, **22**(5), 595-616